Transport specificity of FpvA and FpvB for pyoverdine–antibiotic conjugates in Pseudomonas aeruginosa

Johan Revol-Tissot, Christine Cézard, Anne Forster, Hélène Puja, Françoise Hoegy, Isabelle J. Schalk, Gaëtan L.A. Mislin, Benjamin Bouvier, Coraline Rigouin

PII: S0968-0896(26)00190-2

DOI: https://doi.org/10.1016/j.bmc.2026.118734

Reference: BMC 118734

To appear in:

Received date: 20 February 2026

Revised date: 11 June 2026

Accepted date: 23 June 2026

Please cite this article as: J. Revol-Tissot, C. Cézard, A. Forster, et al., Transport specificity of FpvA and FpvB for pyoverdine–antibiotic conjugates in Pseudomonas aeruginosa, (2026), https://doi.org/10.1016/j.bmc.2026.118734

Transport Specificity of FpvA and FpvB for Pyoverdine–Antibiotic Conjugates in *Pseudomonas aeruginosa*

Johan Revol-Tissot[1,2], Christine Cézard[3], Anne Forster[1,2], Hélène Puja[1,2], Françoise Hoegy[1,2], Isabelle J. Schalk[1,2], Gaëtan L. A. Mislin[1,2]*, Benjamin Bouvier[4]*, Coraline Rigouin[1,2]*

[1] CNRS, University of Strasbourg, UMR7242, UMR7242, ESBS, Bld Sébastien Brant, F-67412 Illkirch, Strasbourg, France.

[2] University of Strasbourg, UMR7242, ESBS, Bld Sébastien Brant, F-67412 Illkirch, Strasbourg, France.

[3] Laboratoire de Glycochimie et des Agroressources d'Amiens (LG2A), UR 7378, Université de Picardie Jules Verne, UFR des Sciences, 33 Rue St Leu, 80000 Amiens, France.

[4] Enzyme and Cell Engineering, CNRS UMR 7025/Université de Picardie Jules Verne, 10 Rue Baudelocque, 80039 Amiens Cedex, France.

*Corresponding authors: rigouin@unistra.fr and benjamin.bouvier@u-picardie.fr and mislin@unistra.fr

ORCID		
	Johan Revol-Tissot	0009-0002-6203-5498
	Christine Cézard	0000-0003-3772-6465
	Anne Forster	0009-0007-4072-3579
	Hélène Puja	0000-0002-9974-547X
	Françoise Hoegy	0000-0002-5440-5818
	Isabelle, J. Schalk	0000-0002-8351-1679
	Gaëtan L.A. Mislin	0000-0002-5646-3392
	Benjamin Bouvier	0000-0001-8782-2426
	Coraline Rigouin	0000-0001-8704-1638

Abstract

Pyoverdines (PVDs) are fluorescent siderophores produced by many *Pseudomonas* species. In *P. aeruginosa,* the TonB-dependent transporters (TBDT) FpvA and FpvB mediate PVD-dependent iron acquisition. PVDs have emerged as promising vectors for antibiotics in antibacterial Trojan horse strategies. However, the uptake of PVD-antibiotic conjugates by FpvA and FpvB remains poorly characterized. Here, we report the semisynthesis of a PVD–oxazolidine conjugate used as a molecular tool to investigate how *P. aeruginosa* accesses iron via these TBDTs in the presence of two native PVDs and their corresponding antibiotic conjugates. Growth assays demonstrate that *P. aeruginosa* can access iron chelated by PVDs through both FpvA and FpvB. In contrast, although both antibiotic conjugates provide iron to the strain via FpvA, only one does so via FpvB, indicating differential receptor recognition. Docking analyses reveal that native PVDs adopt similar binding modes within both FpvA and FpvB. However, FpvB—previously described as a broadly selective transporter—exhibits selective restriction toward PVD–antibiotic conjugates. Our results provide insights for the design of PVD-antibiotic conjugates and emphasize the critical role of the conjugation site on PVD in ensuring efficient transporter-mediated uptake.

Keywords : Pyoverdine*,* oxazolidinone, sideromycin, siderophore, *Pseudomonas aeruginosa*, TonB-dependent transporters, iron uptake systems.

1. Introduction

Antimicrobial Resistance (AMR) is the major health challenge of the forthcoming decades.[1] The discovery of innovative antibacterial strategies is therefore an urgent necessity, especially against Gram-negative pathogens responsible for severe infections and for which only scarce therapeutic options still remain. *Pseudomonas aeruginosa* is one of these critical bacteria. The outer membrane of *P. aeruginosa* constitutes a major permeability barrier that limits the passive diffusion of many antibiotics.[2] Three main strategies enable molecules to cross the outer membrane of Gram-negative bacteria : (i) diffusion through the lipid bilayer for small hydrophobic compounds, (ii) passive diffusion through porins for small hydrophobic molecules, and (iii) active transport via TonB dependent transporters (TBDTs) for compounds such as siderophores, small molecules having a very high affinity for iron and involved in the acquisition by bacteria of this nutrient.[3,4]

Iron is a crucial and non-metabolically substitutable nutrient for bacteria. In aerobic conditions and at physiological pH, iron(III) is poorly soluble and, due to nutritional immunity (iron sequestration by proteins) in humans, the concentration of iron(III) available to pathogens is estimated to range from 10^{-18} to 10^{-24} M.[5] To fulfill their need for iron, bacteria use siderophores. These compounds are synthesized by the bacteria and secreted into the extracellular environment to strongly chelate iron(III). The resulting ferric complex is then specifically recognized by TBDTs, which mediates its translocation into the periplasm using energy derived from the TonB machinery.[3,6,7]

P. aeruginosa produces two siderophores, pyochelin (PCH) and pyoverdine (PVD).[8,9] Pyoverdines are fluorescent siderophores produced by many *Pseudomonas* species. They share a conserved dihydroxyquinoline chromophore linked to a variable peptide chain containing two hydroxamate groups that ensure Fe(III) hexacoordination. The peptide moiety is highly variable, with over 500 PVD structures identified.[10,11] Each *P. aeruginosa* strain produces only a single PVD and expresses a specific TBDT for the uptake of its corresponding ferric PVD complex. While strains typically use their own PVD for iron acquisition due to transporter specificity, cross-feeding can occur.[10] For instance, *P. aeruginosa*

ATCC 15692 (PAO1) which naturally produces PVD **2**, can utilize PVD **1** from *P. fluorescens* ATCC13525 (Figure 1).

In *P. aeruginosa* PAO1, ferri-PVD **2** uptake into the periplasm is mediated by the TBDTs FpvA and FpvB, with FpvA acting as the primary transporter.[10,12,13,14] Iron is released in the periplasm, and apo-PVD is recycled back to the extracellular medium.[15,16] Because ferric PVD is actively transported into the periplasm, this system can be exploited to deliver PVD–antibiotic conjugates using a Trojan Horse strategy.[17]

The total synthesis of PVDs remains a significant scientific challenge, and only a few approaches have been reported to access these molecules or relevant analogs.[18,19] Therefore, semisynthesis has become the strategy of choice for preparing sideromycins, which are antibiotics covalently linked to PVD-based siderophores. In this approach, the intricate scaffold of the siderophore is produced by bacteria, extracted from the culture broth, purified and subsequently conjugated to the antibiotic using a short organic synthesis.[20,21] This semisynthesis strategy represents a greener approach, combining the efficiency of biosynthesis with the versatility of organic synthesis. Recent developments in enzymatic engineering applied to Non Ribosomal Peptide Synthetase (NRPS) has led to the bioproduction of PVD analogs.[22–24] In this context, our group reported the enzymatic engineering of the adenylation domain of the NRPS PvdD, leading to the production of PVD **3** bearing an azide function when the *P. aeruginosa* NRPS mutant was cultivated in the presence of 4-azido-L-homoalanine (4-azHA) (Figure 1).[25] Azide **3** was used as starting material in the semisynthesis of conjugate PVD-oxazolidinone **4**. Conjugate **4** was shown to chelate iron(III) and to provide iron to the bacteria via the PVD-dependent iron uptake pathway.[25] The lack of antibacterial activity reported for conjugate **4** could be explained by the in vivo stability of the disulfide bond bridging the siderophore vector and the antibacterial payload. Indeed, previous studies have shown that when using siderophore vectors with a periplasmic target, the oxazolidinone antibiotic must be released from the conjugate into the periplasm in order to diffuse across the inner membrane and inhibit the translation process in the cytoplasm.[26,27] The absence of disulfide bond cleavage renders conjugate **4** an ineffective sideromycin; paradoxically, this limitation

makes it a powerful molecular probe for elucidating the critical requirements for the design of potent PVD-antibiotic conjugates. To this end, we directly compared the ability of *P. aeruginosa* to access iron from conjugates **4** and **5,** two structurally distinct PVD-oxazolidinone conjugates. The semisynthesis of conjugate **5**, derived from *P. fluorescens* PVD **1** (Figure 1) is reported herein. The involvement of the TBDTs FpvA and FpvB in mediating iron acquisition in the presence of conjugates **4** and **5** was investigated by biological assays, and molecular docking studies were performed to support and rationalize the experimental observations.

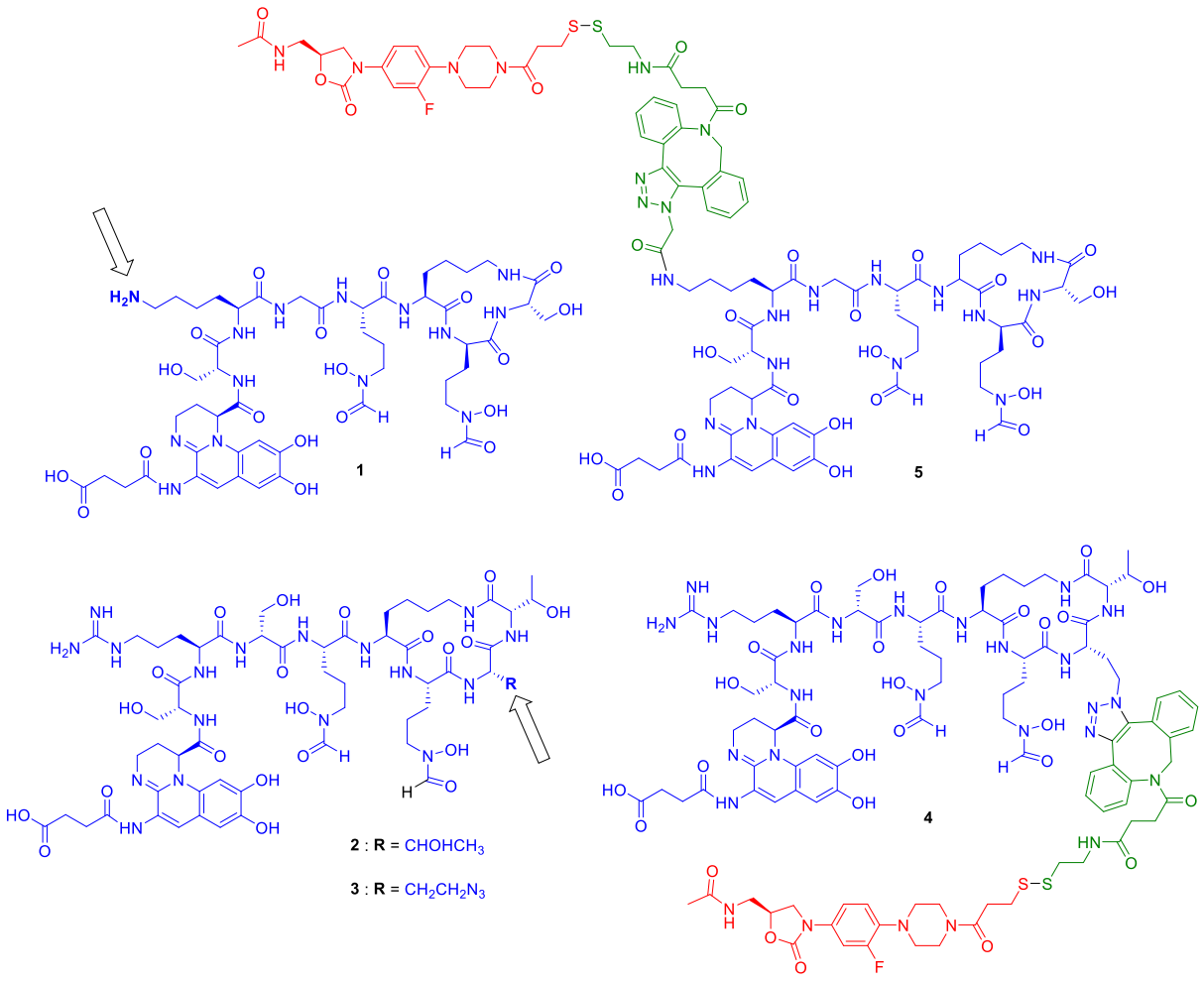

Figure 1. Structures of PVD **1** produced by *P. fluorescens* and of PVD **2** and PVD **3** produced by *P. aeruginosa*. Structure of PVD-oxazolidinone conjugates **4** and **5**. For the sake of clarity PVD structures are colored in blue, the linker is colored in green and the antibiotic is colored in red. Functionalization position on PVD are indicated with black arrows.

2. Results and discussion

2.1. Semisynthesis of a new PVD-oxazolidinone conjugate

Conjugate **5** was prepared by semisynthesis from PVD **1** extracted from a *P. fluorescens* ATCC13525 culture broth. PVD **1** was further purified using Amberlite XAD-4 resin and used directly in the subsequent synthetic steps. The conjugation between PVD **1** and the antibiotic payload was performed using Strain-Promoted Alkyne-Azide Cycloaddition (SPAAC). PVD **1** produced by *P. fluorescens* ATCC13525 bears the terminal primary amine of a lysine side chain, where an azide function could be easily introduced. Moreover, this position was previously shown to be reactive in an acylation reaction and could be functionalized without impairing the recognition by FpvA.[28] An azide function was introduced on PVD **1** using the activated ester strategy. 2-azidoacetic acid **6** was converted to *N*-hydroxysuccinimide ester **7** using EDCI hydrochloride as coupling agent. NHS ester **7** was further reacted with PVD **1** in the presence of triethylamine in a mixture of DMF and water leading to the expected azide-PVD **8**. DBCO derivative **9** and the PVD-azide **8** were reacted in a mixture of DMF and water leading to the expected conjugate **5** isolated in 32% yield over three steps (Scheme 1).

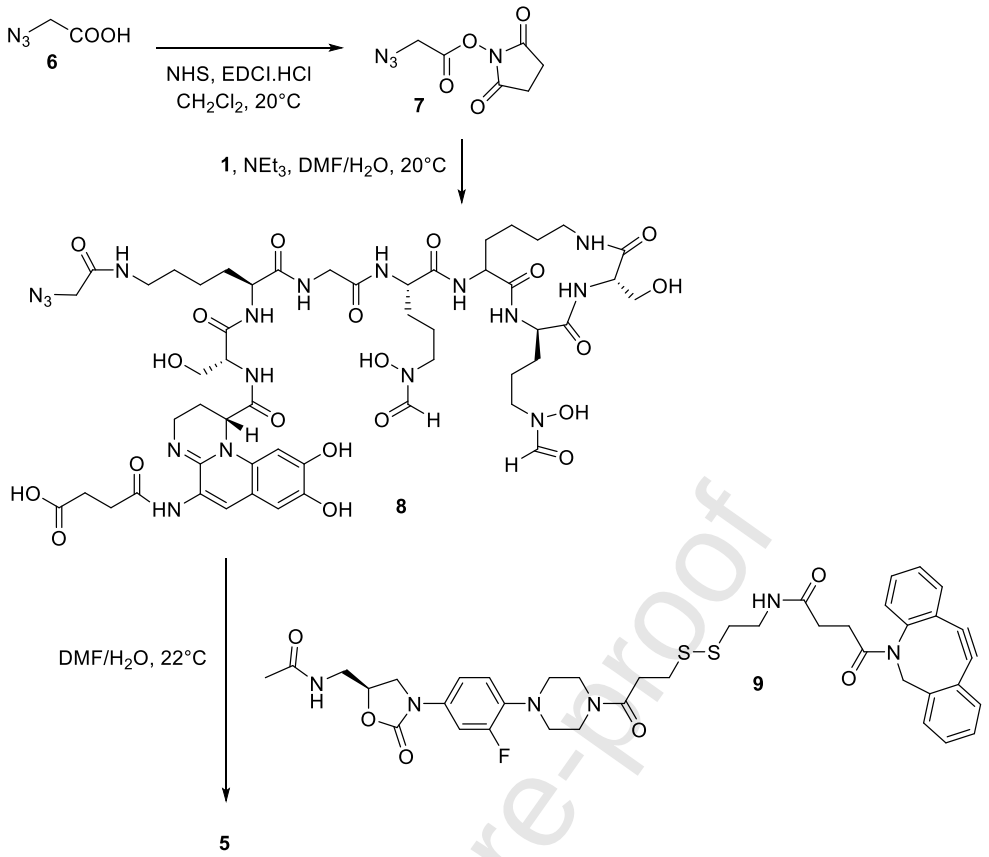

Scheme 1. Synthesis of the PVD-oxazolidinone conjugate **5**.

2.2. Chelation and photophysical properties of conjugate 5

Iron chelation and associated spectral properties of conjugate **5** were evaluated and compared with those of the native PVD **1**. Results of the Chrome-azurol S colorimetric assay gave evidence of similar iron chelation properties between PVD **1** and conjugate **5** (Figure S7). In addition, both molecules exhibited a maximal absorbance at 402 nm at pH 7 (Figure S8 A and B) and a maximal fluorescence emission at 450 nm upon excitation at 402 nm. As for PVD **1**, fluorescence is quenched when iron is chelated (Figure S8 C and D). Overall, this proves that the addition of the antibiotic moiety to PVD **1** via the DBCO-triazole spacer does not affect the iron chelation properties of the molecule, which is known to be crucial for the recognition and transport of the ferri-PVD complex via the PVD-specific transporter FpvA.[10] Interestingly, similar results were obtained for PVD **2** and conjugate **4**.[25]

2.3. Iron acquisition by *P. aeruginosa* PAO1 using PVDs and PVD conjugates

As expected, conjugate **5** showed no antibacterial activity against *P. aeruginosa* PAO1, similar to conjugate **4**,[25] with a minimal inhibitory concentration (MIC) exceeding 512 μM. This suggests that the oxazolidinone moiety is not released from the conjugate. The stability of conjugate **4** was evaluated by mass spectrometry after incubation with the supernatant of a growing *P. aeurignosa* culture. No degradation was detected over time, indicating that the conjugate remained stable during bacterial growth (Figure S9). The lack of antibiotic activity is advantageous, as both conjugates **4** and **5** retain iron-chelating ability, allowing us to investigate how *P. aeruginosa* acquires iron from these two structurally distinct molecules and to identify the TBDT involved in the process. To this end, we performed growth assays under iron-limiting conditions using *P. aeruginosa* mutants unable to synthesize their own siderophores (Δ*pchA*Δ*pvdF),* ensuring that the only siderophores available were those experimentally supplied. The parental strain and the corresponding *fpvA* and *fpvB* deletion mutants were grown in CAA medium supplemented, or not, with 20 μM of either the native PVD or the corresponding conjugates. Under these conditions, iron in the medium is fully chelated by the added siderophores or conjugates, which are present in excess; thus, bacterial iron acquisition relies on the uptake of the ferric–PVD or ferric-conjugate complexes. Growth of PAO1Δ*pchA*Δ*pvdF* strain in the presence of these molecules indicates that they can be used as siderophores, whereas growth inhibition would be expected if the cells were unable to utilize them. Deletion of *fpv*B had no detectable impact on growth in the presence of either PVD **1,** PVD **2** or their corresponding conjugates **5** and **4**, indicating that FpvB is not essential for iron acquisition via these compounds under these conditions (Figures 2A and Figure 2B and 2C).[25] In contrast, deletion of *fpvA* resulted in approximately 25 % and 35 % reductions of bacterial growth after 24h of incubation in the presence of PVD **1** and conjugate **5**, respectively, demonstrating that FpvA plays a major role in iron acquisition via these two compounds (Figures 2A and 2E). Of note, the enhanced growth observed with conjugate **5** is attributed to trace iron contamination encountered during its synthesis, leading to the formation of ferric

complexes of the conjugate. The *fpvA* deletion also impaired growth with PVD **2** (by 20% after 24h of growth) while completely abolishing growth with conjugate **4**, indicating that iron acquisition via conjugates **4** relies only on the TBDT FpvA and not FpvB (Figure 2F).[25] Finally, no growth was observed for PAO1Δ*pchA*Δ*pvdF*Δ*fpvA*Δ*fpvB* with any of the tested molecules (Figure 2D).[25] This confirms that iron uptake mediated by PVDs and their conjugates relies exclusively on these two TBDTs. FpvA is the main transporter enabling *P. aeruginosa* to access iron chelated by PVD **1**, conjugate **5**, and PVD **2**, whereas FpvB provides partial redundancy. In contrast, iron acquisition from conjugate **4** relies exclusively on FpvA, as deletion of *fpvA* completely abolishes bacterial growth under these conditions. This marked difference in the ability of *P. aeruginosa* to access iron via FpvB from conjugate **5**, but not from conjugate **4**, is intriguing, particularly since no such disparity is observed when iron is chelated by PVD **1** or PVD **2**. Moreover, FpvB has been described as a broad-specificity hydroxamate-type transporter displaying higher affinity for ferrichrome and ferrioxamine B than for PVD.[14,29]; however, our findings indicate that this TBDT can also exhibit selectivity with respect to chemical modifications of PVDs. To corroborate this experimental hypothesis and gain further insight into the observed behavior, molecular docking studies were conducted to investigate the binding mode of PVDs **1** and **2** and their respective conjugates, **5** and **4**, with the FpvA and FpvB transporters.

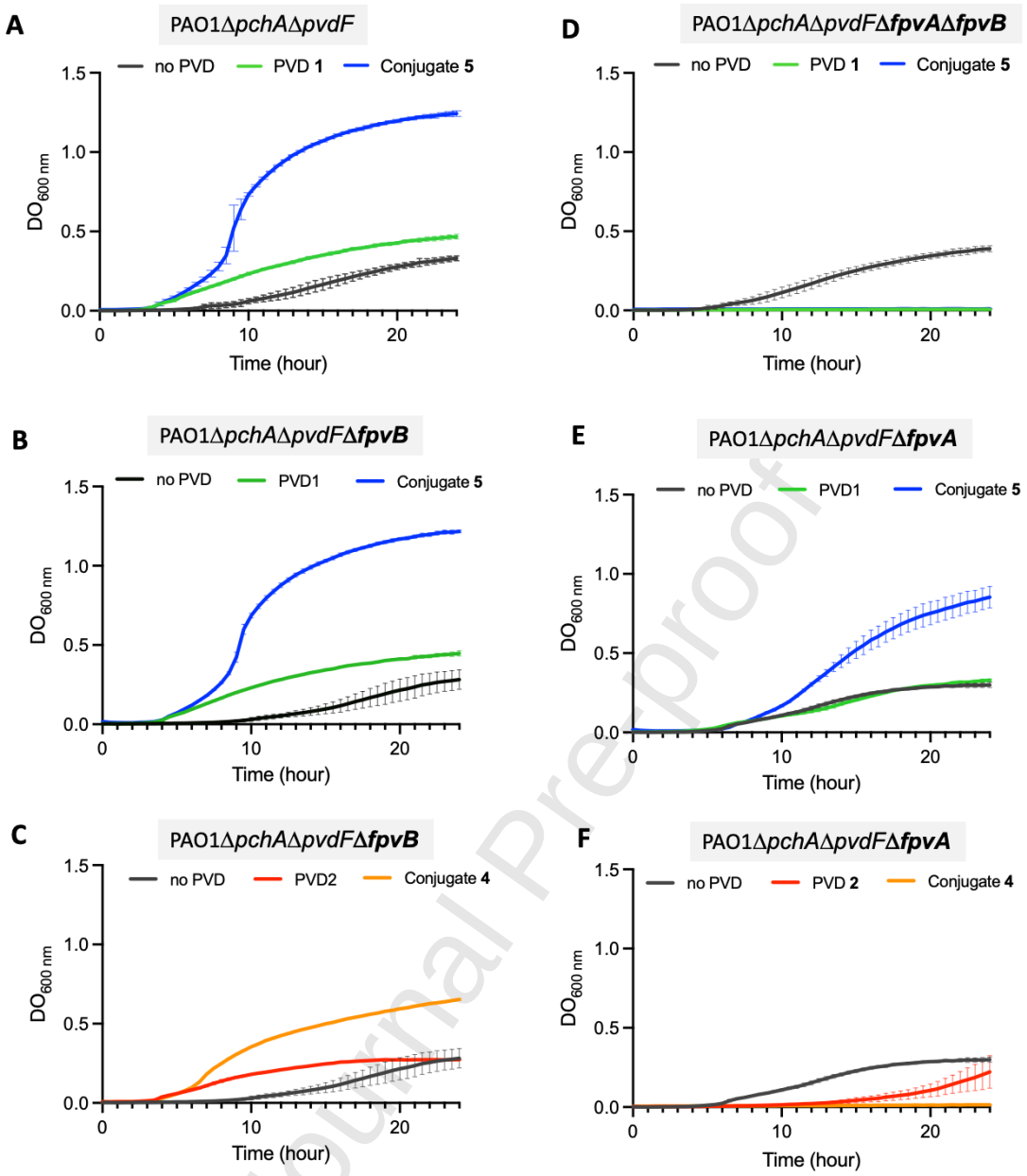

Figure 2. Growth assays in minimal medium CAA of the strains PAO1Δ*pchA*Δ*pvdF* (**A**) PAO1Δ*pchA*Δ*pvdF*Δ*fpvB* (**B** and **C**), PAO1Δ*pchA*Δ*pvdF*Δ*fpvA* (**E** and **F**) and PAO1Δ*pchA*Δ*pvdF*Δ*fpvA*Δ*fpvB* (**D**) with no PVD supplementation (black) or in the presence of 20 µM of PVD **1** (green), conjugate **5** (blue), PVD **2** (red) or conjugate **4** (orange).

2.4. Molecular docking supports the incompatibility between conjugate 4 and FpvB

Docking calculations have been performed to predict whether or not (i) PVD **1** and PVD **2** interact with FpvB in the same way they do with FpvA; (ii) conjugates **4** and **5** interact with FpvA and FpvB in the

same way the cognate PVDs do. In their seminal study on the binding of different PVDs to FpvA, Greenwald *et al.* observed that the binding mode of the siderophore chelating groups onto FpvA was much more conserved across PVD variants than that of the peptide chains, whose amino acid sequences vary between PVD strands.[10] Similarly, Chan *et al*. combined docking and site-directed mutagenesis to prove that ferrichrome-Fe^{3+} and desferrioxamine B-Fe^{3+} complexes share similar orientations in their native transporter and in a structure of FpvB obtained using AphaFold2 (doi:10.1038/s41586-021-03819-2).[14] To quantify the similarity of binding modes among all PVDs and transporters, we measured the root-mean-square deviation (RMSD) of the iron chelating groups (shared among all PVDs) after aligning the β-barrel motif of the transporters.

The top-scoring hits for the docking of PVD **1** and PVD **2** onto their native FpvA transporters showed in both cases a near-perfect superimposition with the experimental structure (RMSD <1 Å), validating our docking strategy. This was further confirmed by cross-docking each PVD onto its non-cognate FpvA transporter, which yielded similar results in terms of both RMSD values and docking scores. When docked in all FpvB models selected from AlphaFold (Figure S10), both PVD **1** and PVD **2** adopted the same orientation as in FpvA, but with a slight shift in the position of the chelating center (RMSD≈3 Å, – Figure S11). We attribute this to the fact that, because the transporter conformation is frozen in the docking calculations, its binding site is not preorganized to accommodate a PVD. Nonetheless, FpvB remains able to preserve the arrangement of the chelating centers of PVD **1** and PVD **2** and is therefore likely to transport them, in agreement with our experimental results (Figure S11).

Docking of conjugates **4** and **5** into FpvA resulted in top-scoring structures whose respective RMSDs to PVD **2** and PVD **1** were below 1 Å (Figure S12). Considering that our experimental findings have shown that these conjugates provide iron to the cell via FpvA, these docking results reinforce the assumption that PVD recognition and transport mainly depend on the recognition and binding of the ferric center. When docked in FpvB, conjugate **5** showed a binding mode similar to those of PVD **1** and PVD **2** (Figure 3). On the other hand, for conjugate 4, the first pose to show an arrangement of the complexing center remotely comparable to the experimental one in FpvA (RMSD: 3.3 Å) was ranked in the final half of

docking solutions, with scores of ~-7 kcal mol-1 compared to ~-12 kcal mol-1 for the group of best solutions which feature a completely different binding mode (average RMSD: 9.5±2.2 Å – Figure 3). This result was consolidated by running five independent docking runs on each of four different structures of FpvB with different conformations of the flexible lid loops. Quoting Greenwald *et al.*:[10] "The specificity of the ferric–pyoverdine binding site of FpvA is conferred by the structural elements common to all ferric–pyoverdines, i.e. the chromophore, iron, and its chelating groups". Provided this assumption also holds true for FpvB, our docking calculations explain the experimentally observed inability of *P. aeruginosa* to access iron from conjugate **4** by the failure of this conjugate to bind in the canonical arrangement. Indeed, due to the orientation of the oxazolidinone moiety, conjugate **4** in FpvB is much more compact than in FpvA and stabilized by different contacts with the transporter: lost contacts with the L7 loop are replaced by new ones with the plug domain, possibly blocking the usual transport mechanism (Figure 3). Considering FpvB's standing as a promiscuous transporter of multiple chemically distinct ligands,[14] its more restrictive selectivity on antibiotic derivatives compared to FpvA is striking. Although the PVDs and their grafted linezolids are treated as flexible molecules within the docking framework, the transporter conformations are considered rigid. This rather crude approximation, coupled with the unavailability of an experimental structure for FpvB, might hinder the accuracy of binding predictions on FpvB compared to FpvA despite our use of several FpvB structures with different lid loop conformations. However, the length of the transporter lid loops and their unstructured nature, together with the plasticity of the PVD-linezolids, create a conformational space which is too large to be exhaustively explored using fully flexible docking approaches or even sub-microsecond molecular dynamics simulations governed by pure Boltzmann sampling; the absence of explicit lipid and water molecule would also compromise the realism of lid loop conformations in flexible docking approaches. As such, the added computational cost inherent to these methods would not guarantee more accurate results than our simpler approach. Several aspects also point to a relative agnosticism regarding the positioning of the PVD derivatives with respect to the loops, which support our strategy: (i) the cross-docking of PVDs **1** and **2** to their non-cognate transporters confirms

established experimental results; (ii) the FpvB structure generated via AlphaFold (hence with no PVD-compatible pre-organization of the lid loops) binds its cognate PVD in its experimental position as the optimal docking solution, similar to the behavior observed by Chan et al on ferrichrome-Fe^{3+} [14] (iii) previous work from our group revealed an excellent agreement between a comparable docking methodology and accurate, long-timescale, enhanced sampling (non-Boltzmann) molecular dynamics simulations on FpvA/PVD complexes.[30]

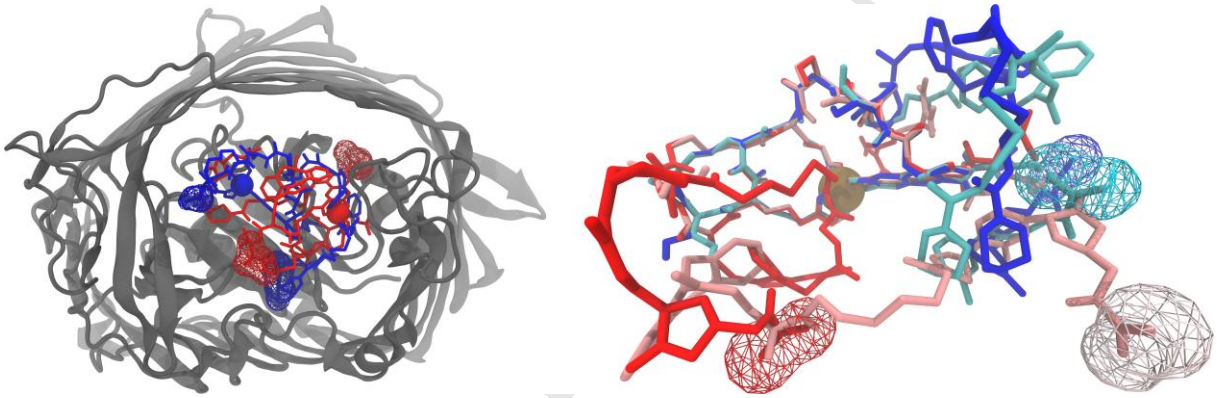

Figure 3. Left: conjugate **4** (red) and conjugate **5** (blue) docked inside FpvB (gray); the Fe^{3+} ions are represented as spheres. PVD atoms involved in FpvB contacts that differ between both PVDs are highlighted using wireframe. **Right:** conformations of conjugate **4** as docked in FpvA (pink) and FpvB (red), and conjugate **5** as docked in FpvA (cyan) and FpvB (blue). All conformations were aligned on the Fe^{3+} (brown sphere) chelating center. Atoms at the end of the antibiotic chain are highlighted as wireframe, bringing out the different orientations of this chain for the two conjugate **4** structures.

3. Conclusion

The launch of cefiderocol has demonstrated the real potential of siderophore-antibiotic Trojan horse conjugates in the fight against resistant bacterial pathogens.[31] However, despite extensive efforts in the field[32–35], molecular determinants governing the recognition and transport of siderophore-antibiotic conjugates by their cognate transporters remain poorly understood. The work presented herein demonstrates that the site of antibiotic attachment within the PVD scaffold is a critical

determinant of transporter recognition. Our experimental data, supported by docking studies, show that conjugation of an oxazolidinone antibiotic to either the N- or C-terminal region of type I PVD does not alter its positioning within the plug domain of FpvA, the main PVD transporter of *P. aeruginosa*. In contrast, transport through FpvB is more sensitive to the position of the conjugated antibiotic. While docking models reveal binding modes of the native PVDs comparable to those observed in FpvA, our results indicate that certain PVD-antibiotics conjugates, including compounds **4**, are less efficiently recognized by FpvB. These findings highlight the importance of considering not only siderophore recognition by the primary transport but also the ability of conjugates to exploit secondary uptake pathways. The capacity of PVD-antibiotic conjugates to utilize two TBDTs is likely to enhance activity across heterogenous clinical isolated and reduce the risk of resistance arising from alterations in a single transport route.[36] Overall, this study establishes that precise control over the site of antibiotic attachment is essential for preserving optimal transporter-mediated uptake. More broadly, it provides a framework for the rational of PVD-based Trojan horse antibiotics and underscores the value of enzyme engineering approaches for generated tailored siderophore vectors with optimal TBDT recognition.[37,38]

4. Experimental

4.1. Chemicals. Oxazolidinone-DBCO compound **9** and conjugate **4** were prepared as previously described.[25] *N*-hydroxysuccinimide (NHS) and azidoacetic acid **6** were purchased from Tokyo Chemical Industry (TCI) Europe (Zwijndrecht, Belgium). PVD **1** was extracted from broth according the procedure described in supportive information. All reagents and solvents were purchased from Sigma-Aldrich (Saint Louis, MO, USA), TCI (Tokyo, Japan) or Fisher Scientific (Loughborough, UK). All chemicals were used as received, unless otherwise stated. All reactions were carried out under argon (technical quality, Air products, Aubervilliers, France). Solvents used were of analytical grade purity (>99.9%). When necessary, solvents and bases were purchased extra-dry.

4.2. Chromatographic analysis and purification. High-Performance-Liquid-Chromatography (HPLC) were performed using preparative HPLC LaPrep Sigma (VWR, Leuven, Belgique) and L3104 detector with UV-vis detection at 214 nm, 254 nm, 280 nm and 400 nm. To perform HPLC, preparative HPLC column Waters XBridge Peptide BEH300 C-18 reverse-phase column (19 mm x 150 mm; 5 µm; flow rate: 4.0 mL/min; pore size 130 Å) was used. The column was purchased from Waters (Guyancourt, France).

4.3. Mass spectrometry analysis and HPLC-MS. Mass spectra were acquired on a time-of-flight mass spectrometer (MALDI-TOF-TOF Autoflex Speed LRF, Bruker Daltonics, Bremen, Germany) equipped with a nitrogen laser (λ = 337 nm). An external multi-point calibration was carried out before each measurement using the singly charged peaks of a standard peptide mixture (0.4 µM, in water acidified with 1% HCOOH). Accumulation and data processing were performed with FlexAnalysis 3.0 software. The α-cyano-4-hydroxy-cinnamic acid (HCCA) matrix was obtained from Sigma (St Louis, MO, USA). Matrix solutions were freshly prepared: HCCA was dissolved to saturate in a $H_2O/CH_3CN/HCOOH$ (50/49/1) solution. Typically, a 1/1 mixture of the sample solution was mixed with the matrix solution and 1 µL of the resulting mixture was deposited on the stainless-steel plate. Analytical HPLC-MS was performed using a LC 1200 Agilent with quadrupole-time-of-flight (QTOF) (Agilent Accurate Mass QToF 6520) with a Zorbax Agilent C18-column (C18, 50 mm x 2.1 mm; 1.8 µm) using the following parameters: The solvent system: A (acetonitrile + 0.05% formic acid) and B (H_2O + 0.05% formic acid); Gradient (Tmin,(%B)): T0 (98%), T4(0%), T8(0%), T8.1(98%). Flow rate of 0.5 mL/min; Column temperature: 40°C; DAD scan from 190 nm to 700 nm. Ionization mode : ESI^+.

4.4 PVD 1 production. The *Pseudomonas fluorescens* ATCC13525 strain was initially cultivated overnight in 5 mL of LB medium at 30°C with orbital stirring at 220 rpm. The following day, the cultures were centrifuged at 8500 rpm for 5 minutes, and the bacterial pellets were resuspended in casamino acid (CAA) medium consisting of casamino acids (5 g/L), K_2HPO_4, $3H_2O$ (1.46 g/L), and $MgSO_4$, $7H_2O$ (0.25 g/L). CAA medium reagents were successively obtained from Gibco (Detroit, MI, USA), Merck

(Darmstadt, Germany) and ITW Reagents (Darmstadt, Germany). The bacterial cells were washed twice with fresh CAA medium. A second overnight culture was then initiated in 5 mL of CAA at 30°C with orbital shaking at 220 rpm. The next day, cultures were again centrifuged at 8500 rpm for 5 mn, and the bacterial pellets were resuspended in 5 mL of CAA medium. The bacterial suspensions were then diluted 1:200 into 1 L of fresh CAA medium. This volume was distributed into two Erlenmeyer flasks and incubated at 25°C with orbital stirring at 220 rpm for 48 h. After incubation, cultures were centrifuged at 8000 rpm for 20 mn, and the supernatants were collected and pooled. The pooled supernatant was sterilized twice using Stericup® Quick Release vacuum filtration systems equipped with 0.22 µm pore size membranes (EMD Millipore®, Merck, Darmstadt, Germany). Pyoverdine (PVD) production was monitored by measuring absorbance at 400 nm using a UV-Vis SPECORD 2025 spectrophotometer (Analytik Jena, Saint-Aubin, France) with a molar extinction coefficient ε = 19,000 $L \cdot mol^{-1} \cdot cm^{-1}$. The filtered supernatant was then acidified to pH 6 using hydrochloric acid (HCl) solution. Acidification was visibly confirmed by the disappearance of the yellow-green coloration of the supernatant. PVD purification was carried out using Amberlite XAD-4 polymeric resin (Merck, Darmstadt, Germany). The resin was pre-conditioned with 1% HCl in ethanol before the addition of the culture supernatant. PVD was then eluted using 0.1% triethylamine in a 50:50 water/ethanol mixture. The absorbance at 400 nm of the eluted fractions was measured to confirm and quantify the presence of purified PVD. The eluted solution was evaporated under reduced pressure to remove ethanol, and the remaining aqueous phase was freeze-dried for 2 days using a Cosmos freeze dryer (Cryotec, Lunel-Viel, France). The final PVD product was obtained as a yellow powder. From 1 L of *P. fluorescens culture*, we obtained 156 mg of lyophilizate containing PVD compound **1**.

4.5. Synthesis of conjugate 5. 2-azidoacetic acid **6** (6 mg**,** 0.056 mmol) was dissolved in CH_2Cl_2 (1 mL) and 1-ethyl-3-(3-dimethylaminopropyl)carbodiimide hydrochloride (EDCI.HCl) (16 mg, 0.085 mmol) was added to the mixture at 20°C. *N*-hydroxysuccinimide (NHS) (10 mg, 0.085 mmol) was added to the reaction mixture. The resulting solution was stirred under argon at 20°C for 2 days, diluted in CH_2Cl_2 and then washed successively with water and brine before being dried over Na_2SO_4. The desiccant was

filtered off and the solvent was removed under reduced pressure to give the *N*-hydroxysuccinimide (NHS) ester **7** (white powder) used as it is for the next step. In parallel, the extracted PVD **1** (33 mg, 0.028 mmol) was dissolved in a dimethylformamide (DMF)/H_2O (90/10) mixture (2.7 mL/0.3 mL, 3.0 mL final) then triethylamine (0.047 mL, 0.34 mmol) and activated ester **7** (11 mg, 0.056 mmol) were added successively to reaction mixture. The resulting solution was stirred under argon at 20°C for 2 days. Addition of diethyl-ether to the mixture led to the formation of a white precipitate. The suspension was further centrifugated in a 50 mL falcon tube for 10 min at 10°C at 12298 *g* (Eppendorf, Montesson, France). After centrifugation, supernatant was removed and pellet was solubilized in water to be freeze-dried. The expected PVD-azide compound **8** was obtained as a yellow-powder. PVD-azide **8** production was assessed by MALDI-TOF analysis of the crude mixture (Figures S3 and S4). PVD-azide **8** was further used as it without any further purification. PVD-azide **8** (35 mg, 0.028 mmol) was dissolved in a DMF/H_2O (90/10) mixture (3.0 mL/0.33 mL, 3.33 mL final). Oxazolidinone-DBCO compound **9** (22 mg, 0.028 mmol) was added to the mixture and the resulting solution was stirred under argon at 22°C for 2 days. Addition of diethyl-ether to the mixture led to the formation of a white precipitate. The suspension was further centrifugated in a 50 mL falcon tube for 10 min at 10°C at 12298 *g* (Eppendorf, Montesson, France). After centrifugation, supernatant was removed and pellet was solubilized in water to be freeze-dried. The expected PVD-oxazolidinone **6** was obtained as a slight yellow powder. The crude powder was solubilized in an acetonitrile (MeCN)/water miwture containing 0.1% Trifluoroacetic acid (TFA) solution (50/50 for a final volume of 1.5 mL). To perform HPLC, we treated crude PVD-oxazolidinone compound **5** with an iron(III) chloride solution (19.3 µL from 2.175 M stock solution, 0.042 mmol, 28 mM final concentration). The resulting sample was purified by preparative HPLC column Waters XBridge Peptide BEH300 C-18 reverse-phase column (flow rate : 4.0 mL/min) using MeCN containing 0.1% TFA in H_2O (Solvent A) and 0.1% TFA in MeCN/H_2O 9:1 (Solvent B). The fractions were collected using PVD UV-absorbance at 400 nm and 214 nm using 20 minutes gradient B 95% to 5%. The expected PVD-oxazolidinone conjugate **5** (18 mg, 0.009 mmol, yield: 32% over three combined steps) was freeze-dried and obtained as a beige powder.

4.6. Chrome-Azurol S Assay and spectral properties. Iron chelation was assessed by using a colorimetric Chrome-Azurol S (CAS) assay developed by Schwyn and Neilands.[39] Briefly, a CAS solution was prepared (HDTMA 600 µM, CAS 150 µM, anhydrous piperazine 500 mM in HCl 2M) and complexed (CAS) or not (Apo-CAS) with iron from $FeCl_3$ 15 µM solution in HCl 10mM, the solutions were stored in the dark. 4 mM of sulfosalicylic acid was added to reduce the reaction incubation time. In a 96-well microplate, PS, F-bottom (Greiner Bio-One, North America Inc.), 100 µL of the CAS reagent was added, using Apo-CAS as the positive control, and mixed with 100µL of 2, 20 or 200 µM of PVD1 in HEPES 100 mM pH 7.5 (stock solution 10mM dissolved in water) or conjugate **5** in HEPES 100 mM pH 7.5 (stock solution 10 mM dissolved in DMSO/H_2O 50%). The plates were then incubated at 20°C for 30 min in the dark to allow iron removal from CAS by siderophores. Coloration change was determined by measuring absorbance at 630 nm (Infinite M200 Pro microplate reader, TECAN, Männedorf, Switzerland). Spectral properties were evaluated using the same microplate reader using 20 µM of siderophore supplemented with 40 µM $FeCl_3$.

4.7. Growth assay in iron-deficient conditions. To determine the capacity of *P. aeruginosa* strains (table S1) to use PVDs and the conjugates, growth assays were performed in CAA medium (5 g.L-1 CAA (Gibco Bacto Casamino Acids), 1.46 g.L-1 K_2HPO_4 $3H_2O$, and 0.25 g.L-1 $MgSO_4.7H_2O$, containing ~20 nM of iron) in a U-bottom 96 well microplate (Greiner Bio-One, North America Inc.). Strains were grown as followed: a first overnight culture at 30°C, 220 rpm, in 5 mL CAA supplemented by 1 µM $FeCl_3$, followed by a cell washing step (cultures were spin down at 8500 rpm for 5 mn and resuspend in 10 mL CAA) and a second overnight culture in 10 mL CAA medium at 30°C, 220 rpm. Bacteria were then washed, resuspended in CAA medium at an OD600 nm of 0.01 and distributed in the microplate in the presence or absence of 20 µM of the siderophores. The plates were incubated at 30°C, with shaking, in an Infinite M200 Nano Quant microplate reader and bacterial growth was measured at OD600 nm every 30 min for at least 40 h. The presented data are the mean of three biological replicates. The percentage of growth reduction was calculated at 24 h from the OD600nm of strain PAO1ΔpchAΔpvdFΔfpvA relative to that of strain PAO1ΔpchAΔpvdF. To assess the stability of

conjugate **4** during bacterial growth, 10 µM of conjugate **4** was incubated with culture supernatants of PAO1Δ*pchA*Δ*pvdF* grown in CAA medium and analyzed by mass spectrometry. Supernatants were collected at t0, 2 h, 8 h, and 24 h, filtered and incubated for 48 h at 30°C in the presence of 10 µM compound **4**. As a positive control for reduction, conjugate **4** was treated with 10 mM DTT at room temperature. Reaction products were analyzed by MALDI-TOF mass spectrometry.

4.8. Determination of the minimum inhibitory concentration (MIC). The ability of commercial linezolid and conjugate **5** to inhibit bacterial growth was determined in microplate growth assay. The stock solutions of the tested molecules (10 mM in DMSO 100% or DMSO/H_2O 50%) were diluted from 1024 µM to 0.5 µM in CAA medium in a F-bottom 96 well microplate (Greiner Bio-One, North America Inc.). Bacteria were grown as described above and inoculate in CAA medium at an $OD_{600\,nm}$ of 0.0002. The plate was incubated at 30°C without shaking and growth was estimated after overnight.

4.9. Docking methods. Docking calculations of flexible ligands onto rigid FpvA and FpvB transporters were performed with Autodock Vina[40] using default parameters. Structures of FpvA/PVD complexes were taken from the RSCB Protein Data Bank (www.rcsb.org) under accession numbers 2W76 for FpvA-PVD **2** and 2W78 for FpvA-PVD **1**.[10] Structural models of FpvB were taken from the AlphaFold Protein Structure Database (https://alphafold.ebi.ac.uk); four models with pLDDT scores in the 88.5-90.5 range were selected, indicative of a high to very high confidence in the generated structure (see figure S9). The PVD-oxazolidinone conjugates were built based on their cognate PVD structure, using RDKit (https://github.com/rdkit) to generate the oxazolidinone moiety from a SMILES sequence and minimize its energy. Receptors and ligands were parametrized for Autodock Vina using Meeko (https://github.com/forlilab/Meeko.git). For the PVD-oxazolidinone conjugates, docking calculations were repeated five times with different initial conditions (starting structure, random seed, …). The volume sampled during docking was a 30 Å-sided cube centered on the PAO1 binding site and discretized using a 0.375 Å grid spacing. All docking poses with scores within 10% of the top-scoring pose were considered equally likely solutions. Root-mean-square deviation (RMSD) calculations were performed on the

chromophore, iron cation and chelating groups of the PVDs (26 atoms), after aligning the β-barrel motif of the transporters.

Supplementary material

Mass spectra of compound **1**, **8** and **5**. HPLC-MS analysis of **5**. Strains used for this study. Additional figures for the microbiology experiments and the docking study.

Authors information

Corresponding Authors

* **Coraline Rigouin** (CR)– CNRS/Université de Strasbourg UMR7242 Biotechnologie et Signalisation Cellulaire, Institut de Recherche de l'Ecole de Biotechnologie de Strasbourg (IREBS), 300 Boulevard Sébastien Brant, F-67412 Illkirch, Strasbourg, France. ORCID 0000-0002-5646-3392. Email : rigouin@unistra.fr

* **Benjamin Bouvier** (BB) - Enzyme and Cell Engineering, CNRS UMR 7025/Université de Picardie Jules Verne, 10 Rue Baudelocque, 80039 Amiens Cedex, France. ORCID 0000-0001-8782-2426. Email : benjamin.bouvier@cnrs.fr

* **Gaëtan L.A. Mislin** (GLAM)– CNRS/Université de Strasbourg UMR7242 Biotechnologie et Signalisation Cellulaire, Institut de Recherche de l'Ecole de Biotechnologie de Strasbourg (IREBS), 300 Boulevard Sébastien Brant, F-67412 Illkirch, Strasbourg, France. ORCID 0000-0002-5646-3392. Email : mislin@unistra.fr

Authors

Johan Revol-Tissot (JRT)**–** CNRS/Université de Strasbourg UMR7242 Biotechnologie et Signalisation

Cellulaire, Institut de Recherche de l'Ecole de Biotechnologie de Strasbourg (IREBS), 300 Boulevard Sébastien Brant, F-67412 Illkirch, Strasbourg, France. ORCID 0009-0002-6203-5498. Email : revoltissot@unistra.fr

Christine Cézard (CC)**–**Laboratoire de Glycochimie et des Agroressources d'Amiens (LG2A), UR 7378, Université de Picardie Jules Verne, UFR des Sciences, 33 Rue St Leu, 80000 Amiens, France. ORCID 0000-0003-3772-6465. Email : christine.cezard@u-picardie.fr

Anne Forster (AF)–CNRS/Université de Strasbourg UMR7242 Biotechnologie et Signalisation Cellulaire, Institut de Recherche de l'Ecole de Biotechnologie de Strasbourg (IREBS), 300 Boulevard Sébastien Brant, F-67412 Illkirch, Strasbourg, France. ORCID 0009-0007-4072-3579. Email : anne. forster@unistra.fr

Hélène Puja (HP)– CNRS/Université de Strasbourg UMR7242 Biotechnologie et Signalisation Cellulaire, Institut de Recherche de l'Ecole de Biotechnologie de Strasbourg (IREBS), 300 Boulevard Sébastien Brant, F-67412 Illkirch, Strasbourg, France. ORCID 0000-0002-9974-547X. Email : helene.puja@laposte.net

Françoise Hoegy (FH)– CNRS/Université de Strasbourg UMR7242 Biotechnologie et Signalisation Cellulaire, Institut de Recherche de l'Ecole de Biotechnologie de Strasbourg (IREBS), 300 Boulevard Sébastien Brant, F-67412 Illkirch, Strasbourg, France. ORCID 0000-0002-5440-5818. Email : hoegy@unistra.fr

Isabelle J. Schalk (IJS) **–** CNRS/Université de Strasbourg UMR7242 Biotechnologie et Signalisation Cellulaire, Institut de Recherche de l'Ecole de Biotechnologie de Strasbourg (IREBS), 300 Boulevard Sébastien Brant, F-67412 Illkirch, Strasbourg, France. ORCID 0000-0002-5646-3392. Email :

isabelle.schalk@unistra.fr

Credit authorship contribution statement

JRT extracted and purified PVD **1**. JRT did the synthesis of compounds **9** and of conjugate **5**. FH synthesized azides **7** and **8**. GLAM supervised chemical experiments. HP and AF performed cell growth experiments. AF did the CAS and CMI assays. CR supervised biological experiments. CC and BB designed and ran the docking simulations. GLAM and CR found the grants. CR, GLAM, IJS, CC and BB wrote the present article through inputs of all other authors. All authors have given approval to the final version of the manuscript.

Declaration of competing interest

Authors declare no competing interests

Acknowledgments

GLAM and IJS acknowledge the Inter-disciplinary Thematic Institute (ITI) InnoVec (Innovative Vectorization of Biomolecules, IdEx, ANR-10-IDEX-0002), the SFRI (ANR-20-SFRI-0012). CR acknowledge the *Agence Nationale de la Recherche* (ANR) (ANR-20-CE44-0004 and ANR-25-CE44-7023). Authors also acknowledge the *Centre National de la Recherche Scientifique* (CNRS) for general financial support. The calculations presented herein (CC and BB) were performed using HPC resources from the UPJV MatriCS computing platform, co-funded by the European Regional Development Fund (FEDER) and the Hauts-De-France Regional Council. IJS acknowledge Dr. Anne Bonneau and Mrs Sarah Fritsch for mutant construction. GLAM acknowledge Dr. Laurent Raibaut (Biometals and Biological Chemistry team, UMR7177) for his assistance in the purification of the final products.

References

(1) Piddock, L. J. V. Reflecting on the Final Report of the O'Neill Review on Antimicrobial Resistance. *Lancet Infect Dis* **2016**, *16* (7), 767–768. https://doi.org/10.1016/S1473-3099(16)30127-X.

(2) Nikaido, H. Prevention of Drug Access to Bacterial Targets: Permeability Barriers and Active Efflux. *Science* **1994**, *264* (5157), 382–388. https://doi.org/10.1126/science.8153625.

(3) Schalk, I. J.; Mislin, G. L. A.; Brillet, K. Structure, Function and Binding Selectivity and Stereoselectivity of Siderophore-Iron Outer Membrane Transporters. *Curr Top Membr* **2012**, *69*, 37–66. https://doi.org/10.1016/B978-0-12-394390-3.00002-1.

(4) Schalk, I. J.; Perraud, Q. *Pseudomonas aeruginosa* and Its Multiple Strategies to Access Iron. *Environ Microbiol* **2023**, *25* (4), 811–831. https://doi.org/10.1111/1462-2920.16328.

(5) Raymond, K. N.; Dertz, E. A.; Kim, S. S. Enterobactin: An Archetype for Microbial Iron Transport. *Proc Natl Acad Sci U S A* **2003**, *100* (7), 3584–3588. https://doi.org/10.1073/pnas.0630018100.

(6) Schalk, I. J. Bacterial Siderophores: Diversity, Uptake Pathways and Applications. *Nat Rev Microbiol* **2025**, *23* (1), 24–40. https://doi.org/10.1038/s41579-024-01090-6.

(7) Celia, H.; Noinaj, N.; Buchanan, S. K. Structure and Stoichiometry of the Ton Molecular Motor. *Int J Mol Sci* **2020**, *21* (2), 375. https://doi.org/10.3390/ijms21020375.

(8) Cox, C. D.; Rinehart, K. L.; Moore, M. L.; Cook, J. C. Pyochelin: Novel Structure of an Iron-Chelating Growth Promoter for *Pseudomonas aeruginosa*. *Proc Natl Acad Sci U S A* **1981**, *78* (7), 4256–4260. https://doi.org/10.1073/pnas.78.7.4256.

(9) Cox, C. D.; Adams, P. Siderophore Activity of Pyoverdin for *Pseudomonas aeruginosa*. *Infect Immun* **1985**, *48* (1), 130–138. https://doi.org/10.1128/iai.48.1.130-138.1985.

(10) Greenwald, J.; Nader, M.; Celia, H.; Gruffaz, C.; Geoffroy, V.; Meyer, J.-M.; Schalk, I. J.; Pattus, F. FpvA Bound to Non-Cognate Pyoverdines: Molecular Basis of Siderophore Recognition by an Iron Transporter. *Mol Microbiol* **2009**, *72* (5), 1246–1259. https://doi.org/10.1111/j.1365-2958.2009.06721.x.

(11) Meyer, J.-M.; Geoffroy, V. A.; Baida, N.; Gardan, L.; Izard, D.; Lemanceau, P.; Achouak, W.; Palleroni, N. J. Siderophore Typing, a Powerful Tool for the Identification of Fluorescent and Nonfluorescent Pseudomonads. *Appl Environ Microbiol* **2002**, *68* (6), 2745–2753. https://doi.org/10.1128/AEM.68.6.2745-2753.2002.

(12) Cobessi, D.; Celia, H.; Folschweiller, N.; Schalk, I. J.; Abdallah, M. A.; Pattus, F. The Crystal Structure of the Pyoverdine Outer Membrane Receptor FpvA from *Pseudomonas aeruginosa* at 3.6 Angstroms Resolution. *J Mol Biol* **2005**, *347* (1), 121–134. https://doi.org/10.1016/j.jmb.2005.01.021.

(13) Ghysels, B.; Dieu, B. T. M.; Beatson, S. A.; Pirnay, J.-P.; Ochsner, U. A.; Vasil, M. L.; Cornelis, P. FpvB, an Alternative Type I Ferripyoverdine Receptor of *Pseudomonas aeruginosa*. *Microbiology* **2004**, *150* (6), 1671–1680. https://doi.org/10.1099/mic.0.27035-0.

(14) Chan, D. C. K.; Burrows, L. L. *Pseudomonas aeruginosa* FpvB Is a High-Affinity Transporter for Xenosiderophores Ferrichrome and Ferrioxamine B. *mBio* **2022**, *14* (1), e03149-22. https://doi.org/10.1128/mbio.03149-22.

(15) Greenwald, J.; Hoegy, F.; Nader, M.; Journet, L.; Mislin, G. L. A.; Graumann, P. L.; Schalk, I. J. Real Time Fluorescent Resonance Energy Transfer Visualization of Ferric Pyoverdine Uptake in *Pseudomonas aeruginosa.* A Role for Ferrous Iron. *J Biol Chem* **2007**, *282* (5), 2987–2995. https://doi.org/10.1074/jbc.M609238200.

(16) Imperi, F.; Tiburzi, F.; Visca, P. Molecular Basis of Pyoverdine Siderophore Recycling in *Pseudomonas aeruginosa*. *Proceedings of the National Academy of Sciences* **2009**, *106* (48), 20440–20445. https://doi.org/10.1073/pnas.0908760106.

(17) Mislin, G. L. A.; Schalk, I. J. Siderophore-Dependent Iron Uptake Systems as Gates for Antibiotic Trojan Horse Strategies against *Pseudomonas aeruginosa*. *Metallomics* **2014**, *6* (3), 408–420. https://doi.org/10.1039/c3mt00359k.

(18) Mashiach, R.; Meijler, M. M. Total Synthesis of Pyoverdin D. *Org. Lett.* **2013**, *15* (7), 1702–1705. https://doi.org/10.1021/ol400490s.
(19) Antonietti, V.; Boudesocque, S.; Dupont, L.; Farvacques, N.; Cézard, C.; Da Nascimento, S.; Raimbert, J.-F.; Socrier, L.; Robin, T.-J.; Morandat, S.; El Kirat, K.; Mullié, C.; Sonnet, P. Synthesis, Iron(III) Complexation Properties, Molecular Dynamics Simulations and P. Aeruginosa Siderophore-like Activity of Two Pyoverdine Analogs. *Eur J Med Chem* **2017**, *137*, 338–350. https://doi.org/10.1016/j.ejmech.2017.06.010.
(20) Kinzel, O.; Budzikiewicz, H. Synthesis and Biological Evaluation of a Pyoverdin-Beta-Lactam Conjugate: A New Type of Arginine-Specific Cross-Linking in Aqueous Solution. *J Pept Res* **1999**, *53* (6), 618–625. https://doi.org/10.1034/j.1399-3011.1999.00053.x.
(21) Kinzel, O.; Tappe, R.; Gerus, I.; Budzikiewicz, H. The Synthesis and Antibacterial Activity of Two Pyoverdin-Ampicillin Conjugates, Entering *Pseudomonas aeruginosa* via the Pyoverdin-Mediated Iron Uptake Pathway. *J Antibiot (Tokyo)* **1998**, *51* (5), 499–507. https://doi.org/10.7164/antibiotics.51.499.
(22) Calcott, M. J.; Owen, J. G.; Lamont, I. L.; Ackerley, D. F. Biosynthesis of Novel Pyoverdines by Domain Substitution in a Nonribosomal Peptide Synthetase of *Pseudomonas aeruginosa*. *Appl Environ Microbiol* **2014**, *80* (18), 5723–5731. https://doi.org/10.1128/AEM.01453-14.
(23) Calcott, M. J.; Owen, J. G.; Ackerley, D. F. Efficient Rational Modification of Non-Ribosomal Peptides by Adenylation Domain Substitution. *Nat Commun* **2020**, *11* (1), 4554. https://doi.org/10.1038/s41467-020-18365-0.
(24) Messenger, S. R.; McGuinniety, E. M. R.; Stevenson, L. J.; Owen, J. G.; Challis, G. L.; Ackerley, D. F.; Calcott, M. J. Metagenomic Domain Substitution for the High-Throughput Modification of Nonribosomal Peptides. *Nat Chem Biol* **2024**, *20* (2), 251–260. https://doi.org/10.1038/s41589-023-01485-1.
(25) Puja, H.; Bianchetti, L.; Revol-Tissot, J.; Simon, N.; Shatalova, A.; Nommé, J.; Fritsch, S.; Stote, R. H.; Mislin, G. L. A.; Potier, N.; Dejaegere, A.; Rigouin, C. Biosynthesis of a Clickable Pyoverdine via in Vivo Enzyme Engineering of an Adenylation Domain. *Microb Cell Fact* **2024**, *23* (1), 207. https://doi.org/10.1186/s12934-024-02472-4.
(26) Liu, R.; Miller, P. A.; Vakulenko, S. B.; Stewart, N. K.; Boggess, W. C.; Miller, M. J. A Synthetic Dual Drug Sideromycin Induces Gram-Negative Bacteria To Commit Suicide with a Gram-Positive Antibiotic. *J. Med. Chem.* **2018**, *61* (9), 3845–3854. https://doi.org/10.1021/acs.jmedchem.8b00218.
(27) Boyce, J. H.; Dang, B.; Ary, B.; Edmondson, Q.; Craik, C. S.; DeGrado, W. F.; Seiple, I. B. Platform to Discover Protease-Activated Antibiotics and Application to Siderophore–Antibiotic Conjugates. *J. Am. Chem. Soc.* **2020**, *142* (51), 21310–21321. https://doi.org/10.1021/jacs.0c06987.
(28) Schons, V.; Atkinson, R. A.; Dugave, C.; Graff, R.; Mislin, G. L. A.; Rochet, L.; Hennard, C.; Kieffer, B.; Abdallah, M. A.; Schalk, I. J. The Structure-Activity Relationship of Ferric Pyoverdine Bound to Its Outer Membrane Transporter: Implications for the Mechanism of Iron Uptake. *Biochemistry* **2005**, *44* (43), 14069–14079. https://doi.org/10.1021/bi051155s.
(29) Will, V.; Frey, C.; Normant, V.; Kuhn, L.; Chicher, J.; Volck, F.; Schalk, I. J. The Role of FoxA, FiuA, and FpvB in Iron Acquisition via Hydroxamate-Type Siderophores in *Pseudomonas aeruginosa*. *Sci Rep* **2024**, *14* (1), 18795. https://doi.org/10.1038/s41598-024-69152-6.
(30) Bouvier, B.; Cézard, C.; Sonnet, P. Selectivity of Pyoverdine Recognition by the FpvA Receptor of *Pseudomonas aeruginosa* from Molecular Dynamics Simulations. *Phys. Chem. Chem. Phys.* **2015**, *17* (27), 18022–18034. https://doi.org/10.1039/C5CP02939B.
(31) Sato, T.; Yamawaki, K. Cefiderocol: Discovery, Chemistry, and In Vivo Profiles of a Novel Siderophore Cephalosporin. *Clin Infect Dis* **2019**, *69* (Suppl 7), S538–S543. https://doi.org/10.1093/cid/ciz826.
(32) Ferguson, A. D.; Braun, V.; Fiedler, H. P.; Coulton, J. W.; Diederichs, K.; Welte, W. Crystal Structure of the Antibiotic Albomycin in Complex with the Outer Membrane Transporter FhuA. *Protein Sci* **2000**, *9* (5), 956–963. https://doi.org/10.1110/ps.9.5.956.

(33) Moynié, L.; Hoegy, F.; Milenkovic, S.; Munier, M.; Paulen, A.; Gasser, V.; Faucon, A. L.; Zill, N.; Naismith, J. H.; Ceccarelli, M.; Schalk, I. J.; Mislin, G. L. A. Hijacking of the Enterobactin Pathway by a Synthetic Catechol Vector Designed for Oxazolidinone Antibiotic Delivery in *Pseudomonas aeruginosa*. *ACS Infect Dis* **2022**, *8* (9), 1894–1904. https://doi.org/10.1021/acsinfecdis.2c00202.

(34) Cao, M.; Huynh, M.; Josts, I.; Lao, Y.; Dang, H. H.; Marlin, A.; Huang, X.; Tidow, H.; Boros, E. Covalent Chemical Tagging of Transmembrane Transport Proteins Illuminates the Internalization Pathways of Xenosiderophores. *J. Am. Chem. Soc.* **2026**. https://doi.org/10.1021/jacs.6c00632.

(35) Cao, M.; Huynh, M.; Josts, I.; Lao, Y.; Dang, H. H.; Marlin, A.; Huang, X.; Tidow, H.; Boros, E. Covalent Chemical Tagging of Transmembrane Transport Proteins Illuminates the Internalization Pathways of Xenosiderophores. *J. Am. Chem. Soc.* **2026**, *148* (20), 20509–20519. https://doi.org/10.1021/jacs.6c00632.

(36) Kriz, R.; Spettel, K.; Pichler, A.; Schefberger, K.; Sanz-Codina, M.; Lötsch, F.; Harrison, N.; Willinger, B.; Zeitlinger, M.; Burgmann, H.; Lagler, H. In Vitro Resistance Development Gives Insights into Molecular Resistance Mechanisms against Cefiderocol. *J Antibiot* **2024**, *77* (11), 757–767. https://doi.org/10.1038/s41429-024-00762-y.

(37) Puja, H.; Mislin, G. L. A.; Rigouin, C. Engineering Siderophore Biosynthesis and Regulation Pathways to Increase Diversity and Availability. *Biomolecules* **2023**, *13* (6), 959. https://doi.org/10.3390/biom13060959.

(38) Telfer, T. J.; Richardson-Sanchez, T.; Gotsbacher, M. P.; Nolan, K. P.; Tieu, W.; Codd, R. Analogues of Desferrioxamine B (DFOB) with New Properties and New Functions Generated Using Precursor-Directed Biosynthesis. *Biometals* **2019**, *32* (3), 395–408. https://doi.org/10.1007/s10534-019-00175-7.

(39) Schwyn, B.; Neilands, J. B. Universal Chemical Assay for the Detection and Determination of Siderophores. *Anal Biochem* **1987**, *160* (1), 47–56. https://doi.org/10.1016/0003-2697(87)90612-9.

(40) Eberhardt, J.; Santos-Martins, D.; Tillack, A. F.; Forli, S. AutoDock Vina 1.2.0: New Docking Methods, Expanded Force Field, and Python Bindings. *J. Chem. Inf. Model.* **2021**, *61* (8), 3891–3898. https://doi.org/10.1021/acs.jcim.1c00203.

Transport Specificity of FpvA and FpvB for Pyoverdine–Antibiotic Conjugates in *Pseudomonas aeruginosa*

Johan Revol-Tissot[1,2], Christine Cézard[3], Anne Forster[1,2], Hélène Puja[1,2], Françoise Hoegy[1,2], Isabelle J. Schalk[1,2], Gaëtan L. A. Mislin[1,2]*, Benjamin Bouvier[4]*, Coraline Rigouin[1,2]*

Declaration of interest statement

The authors declare no conflict of interest.

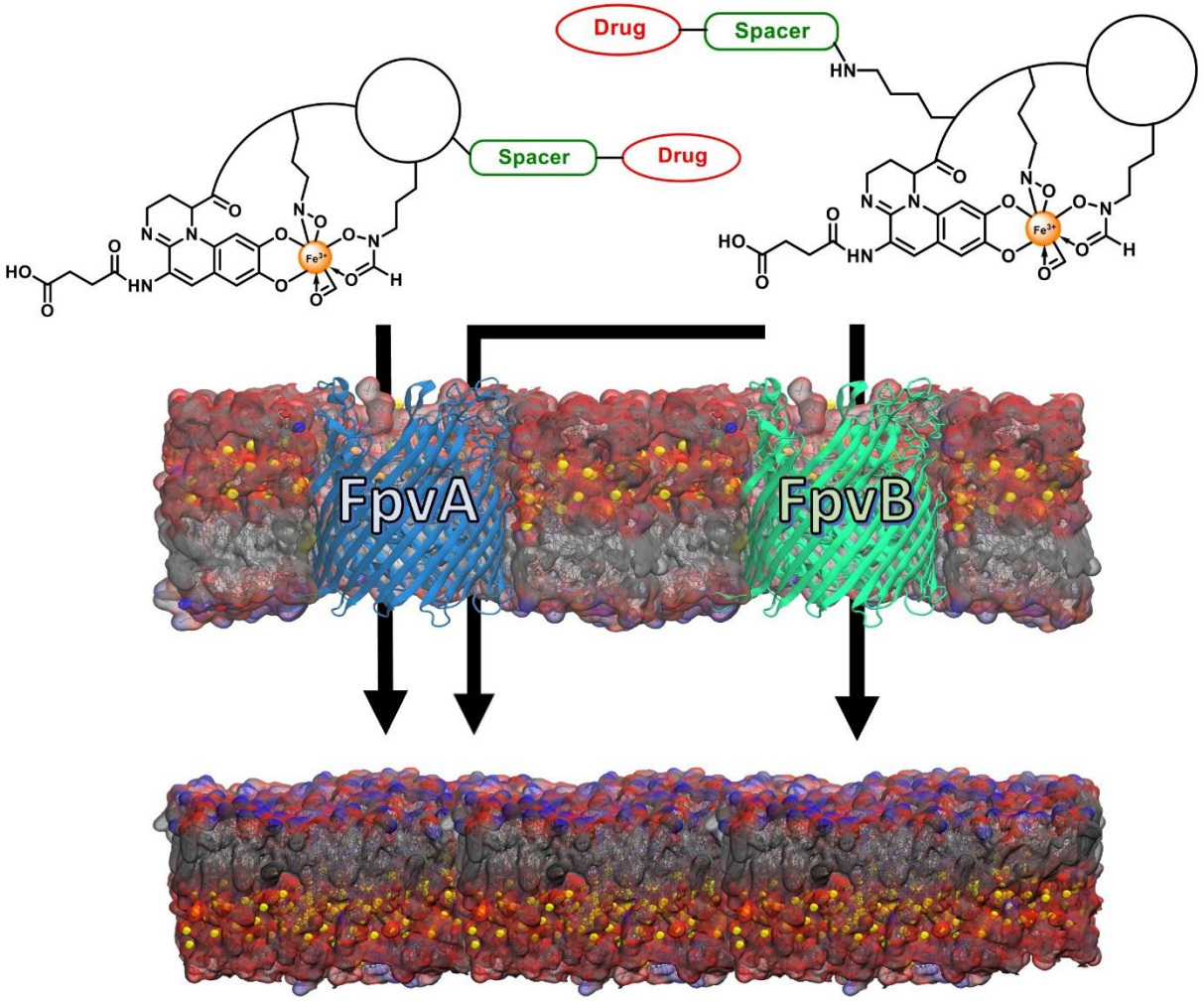

Highlights

• Semisynthesis of a PVD–oxazolidine conjugate enables investigation of siderophore mediated transport in P. aeruginosa.

• Biological assays demonstrate differential iron acquisition from native PVDs and antibiotic conjugates via FpvA and FpvB.

• Docking analyses reveal similar binding modes of native PVDs but selective restriction of PVD–antibiotic conjugates by FpvB.

• The conjugation site on PVD critically governs TBDT-mediated uptake, informing the rational design of Trojan horse antibiotics.